ChemComm

COMMUNICATION

View Article Online
View Journal | View Issue

Cite this: *Chem. Commun.*, 2018, **54**, 13539

Received 2nd August 2018,
Accepted 29th October 2018

DOI: 10.1039/c8cc06301j

rsc.li/chemcomm

Zinc clasp-based reversible toolset for selective metal-mediated protein heterodimerization†

Anna Kocyła and Artur Krężel *

Considering the complex biological quandaries of the tightly woven networks of biological macromolecules, we present an optimized zinc clasp-based toolset from the CD4 co-receptor and Lck protein tyrosine kinase complex for selective, tight and fully reversible protein heterodimerization ($\log K_{12}$ = 18.6). We demonstrated its utility on CD4-tagged proteins with capture from bacterial lysate and constructed molecular baits using a new small-molecule tether.

Essential cellular processes require sets of interactions between hundreds of proteins organized through the course of evolution in time and space to gain as much specificity as possible to maximize the functionality and precision of such interactions.[1,2] To tether biomolecules, small inducers serve as a template where increased effective molarity of a protein causes chemically induced proximity of the two previously dispersed biomolecules.[3,4] Classification of small-molecule tethers is mostly based on the inducer design and the scaffold to be assembled where bifunctional, intact or sensitizing, photocaged precursor poles provide on-demand targeting (PROTACs, T-REX, coumermycin with bacterial DNA gyrase B subunits, methotrexate with dihydrofolate reductase and rapamycin or FKBP and mTOR4).[2,5–7] Scaffolding approaches have been applied to multi-functional biological processes: activation of transduction or cascade pathways, transcriptional and post-translational control of proteins, proximity sensing, bioscreening and protein nanostructural assembly.[8–12] All of the chemically induced dimerization systems have been struggling with such factors as reversibility, binding equilibria, kinetics, and off-target interactions, as well as size and complexity. Frequently it renders the system inapplicable.[2,13,14]

Chemical inducers of protein interactions vital for many types of actions in the cell are zinc ions (Zn(II)) with a unique combination of properties: high Lewis acidity, high thermodynamic stability, flexible coordination geometry, redox inactivity, rapid substitution rates and a low surface area of protein–protein interaction.[15,16] It makes them suitable for both transient and permanent interactions utilized in structure stabilization, oligomerization, catalysis, triggering conformational changes and cellular signaling.[17–20] Strict control of cellular zinc availability (pM to nM range) makes it suitable in dimerization system engineering and an attractive goal for biotechnology, synthetic, chemical and molecular biology.[21] Current *de novo* or bio-inspired toolsets based on metal-mediated interactions still struggle with specificity or demonstrate too low affinity towards metal ions to be applied as universal systems, which is the main obstacle for all dimerization systems to date.[22–25]

Cell surface receptor proteins interact with several hundred protein partners, many of which are involved in human dysfunctioning. The cluster of differentiation family of co-receptors constituting part of a wide range of signaling pathways provides targets for immunophenotyping of cells.[26] The cytosolic C-terminal tail of the CD4 receptor forms a unique zinc-mediated interaction (zinc clasp) with an N-terminal fragment of non-receptor protein tyrosine kinase (Lck) critical for the initial stage of T cell activation. In this study we used a zinc clasp domain to develop a Zn(II)-mediated protein heterodimerization system (Fig. 1A). NMR structural studies demonstrate that the interfacial zinc clasp scaffold is formed by tetrahedral co-coordination of Zn(II) by two cysteine residues from Lck (C^{20} and C^{23}) and two from CD4 (C^{445} and C^{447}), Fig. 1A.[27] Apart from the energetic cost derived from metal binding, the zinc clasp complex is mostly stabilized by a hydrophobic interface placed in a core between helices (Fig. 1B).[27] High content of acidic and basic residues (Lck and CD4, respectively) enables polar interactions to occur with contribution to the total free energy of metal center formation. Moreover, additional Zn(II)-coordinating residues (C^{422}, H^{424}, H^{449}) may affect the specificity of zinc clasp domain assembly (Fig. 1A). The factor of free Zn(II) and protein subunit concentration should be considered in ternary complex formation, which has been reported for a zinc clasp domain.[28] Biophysical studies performed to date show that short model peptides from Lck and CD4 tend to form both homo- and heterodimeric species typically for short CXXC-containing motifs.[21,29]

Department of Chemical Biology, Faculty of Biotechnology, University of Wrocław, F. Joliot-Curie 14a, 50-383, Wrocław, Poland. E-mail: artur.krezel@uwr.edu.pl

† Electronic supplementary information (ESI) available. See DOI: 10.1039/c8cc06301j

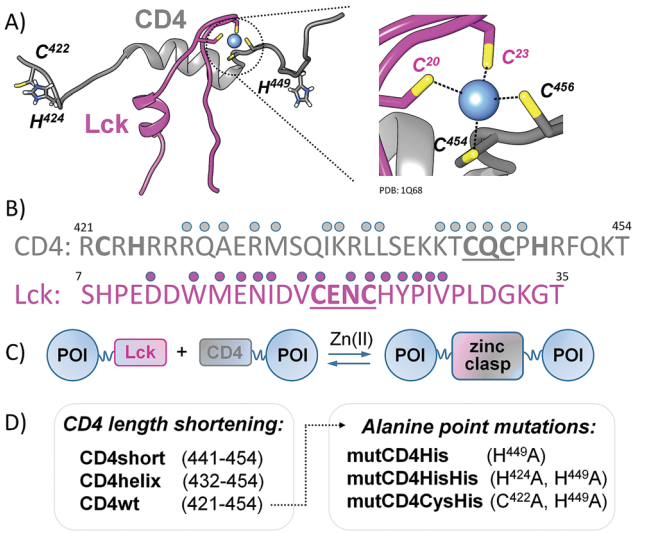

Fig. 1 (A) Zinc clasp scaffold structure with tetrahedral Zn(II) (blue) co-coordination by cysteine residues from CD4 and Lck (PDB: 1Q68). (B) Sequences of wild-type CD4 and Lck peptides. Zn(II)-binding motifs are underlined. Circles indicate amino acid residues responsible for heterodimeric interface interaction (PDBePISA web server).[30] (C) Graphical representation of Zn(II)-mediated, reversible, Point of Interest (POI) heterodimerization with Lck and CD4RARH tags. (D) CD4 peptide models used within the study.

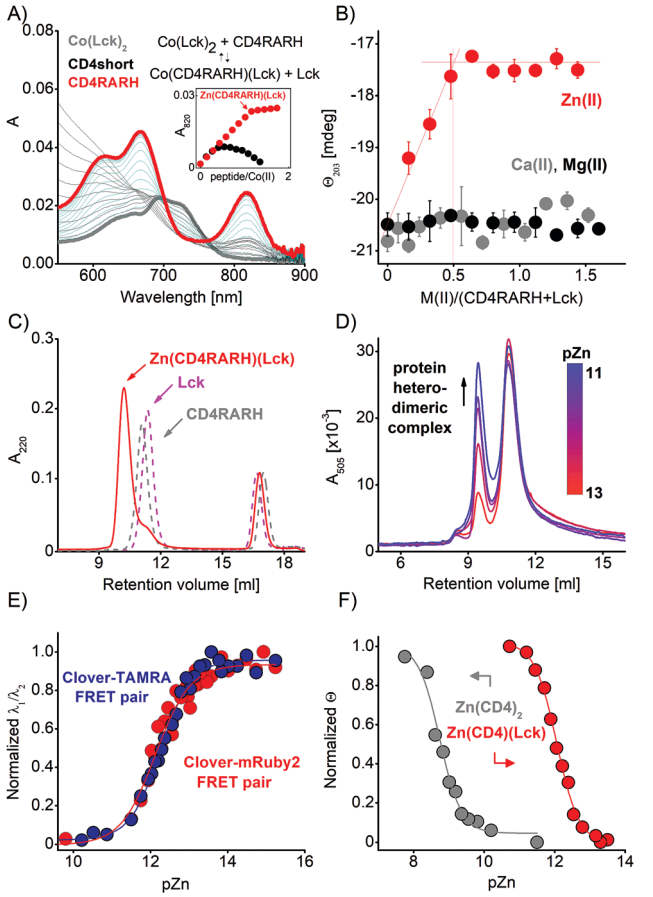

Fig. 2 Heterodimerization, stability, and selectivity of enhanced zinc clasp motif. (A) Spectroscopic reverse titration of $Co(Lck)_2$ complex (grey) with CD4short (black) and CD4RARH (red) peptides. Absorption changes at 820 nm in terms of peptide-to-Co(II) molar ratio (inset). (B) Ellipticity changes of CD4RARH at 203 nm as a function of Zn(II), Ca(II), Mg(II) shown in red, grey, and black, respectively. (C) Size exclusion chromatograms of CD4RARH, Lck and their Zn(II)-mediated hetero-complex. (D) SEC-monitored CD4RARH(Clover) and Lck(mRuby2) complex formation in the Zn(II)-buffered media. (E) FRET-normalized isotherms of the Zn(CD4RARH(Clover))-(Lck(TAMRA)) formation (blue) and Zn(CD4RARH(Clover))(Lck(mRuby2)) (red) as a function of free Zn(II) (pZn = $-\log[Zn(II)]_{free}$) concentration. λ_1/λ_2 ratios were normalized according to the previously published method.[20] (F) CD-monitored isotherms of the $Zn(CD4RARH)_2$ (220 nm) and Zn(CD4RARH)(Lck) (202 nm) formation (grey and red) from equimolar mixture of peptides in a range of free Zn(II) concentration.

Therefore we rationally optimized the CD4 cytoplasmic tail to gain heterodimer selectivity with high femtomolar affinity towards Zn(II) to underpin the need to establish new routes for protein engineering, molecular biology, nanotechnology, *etc.* (Fig. 1C).

Here, we tested three length variants of CD4 to examine the propensity to form monomeric and dimeric species in solution (Fig. 1D and Table S1, ESI†). Peptides were titrated with Zn(II) to monitor changes of LMCT (ligand-to-metal charge transfer) in the UV spectral range, and their affinities for Zn(II) were examined with a chromophoric PAR probe, which competes for Zn(II) with subnanomolar affinity (Fig. S1 and Table S4, ESI†).[31,32] CD4short, CD4helix and Lck form Zn(II)-mediated homodimers, which are too weak to outcompete Zn(II), in contrast to monomeric Zn(CD4wt). Competition of their equimolar mixtures with PAR for Zn(II) indicated the highest affinity of Zn(CD4wt)(Lck) heterodimer with the sharpest inflection point at a peptide-to-Zn(II) molar ratio of 2.0. Because the predomination of heterodimer formation increases with CD4 peptide length, we implemented alanine point mutations of cysteine and histidine residues (beyond the CXC motif) to CD4wt for specificity increase and heterodimer stabilization (Fig. 1D and Table S1, ESI†). Substitution of H^{449} (CD4RCRH) does not affect monomeric complex formation significantly, while lowered stability of the Zn(CD4RCRA) complex has been indicated (Fig. S1, ESI†). Only CD4RARH peptide forms a homodimeric complex along with the lowest affinity for Zn(II). This peptide also demonstrates the highest tendency to form a heterodimeric complex when mixed equimolarly with Lck. Heterodimer conditional binding constant of this complex (K_{12}) determined from PAR competition is 5×10^{18} M^{-2} at pH 7.4 (Table S4, ESI†). To examine heterodimeric species formation more efficiently, spectroscopic analysis with Co(II) as a probe for Zn(II) was employed. Co(CD4)(Lck) complex formation is associated with a red shift of one from three d–d components of the $^4A_2$-to-$^4T_1$(P) transition to 820 nm, without affecting the coordination number (Fig. 2A).[33] Binary and ternary Co(II) complexes have been indicated for all investigated peptides with ε of d–d bands varying from 160 to 900 M^{-1} cm^{-1} (Fig. S2, ESI†). Overlaid spectra of $Co(Lck)_2$ complex titrated with CD4short and CD4RARH peptides confirm the highest heterodimer complex stability of CD4RARH. Furthermore, CD-monitored peptide titrations with Zn(II) specified the most efficient and selective heterodimerization observed for CD4RARH (Fig. S3, ESI†), which was chosen as the most suitable partner for Lck heterodimerization. Selectivity towards the metal ion has been

indicated by CD-monitored titrations with Zn(II), Ca(II) and Mg(II), as presented in Fig. 2B. CD as well as fluorimetric study of equimolar CD4RARH and Lck mixture with Cu(I) indicated different behavior and lack of heterodimer formation (Fig. S4, ESI†).

The enhanced zinc clasp heterodimerization scaffold was characterized by size exclusion chromatography (SEC) of CD4RARH, Lck and their equimolar mixture with Zn(II), where a shift of peaks at 11.5 min to 10 min indicates complex formation (Fig. 2C and Fig. S5, ESI†). To further analyze the equilibria, fluorescently labeled CD4RARH(Clover) with Lck(mRuby2) or Lck(TAMRA) was equimolarly mixed in Zn(II)-controlled (buffered) media (specific amounts of $ZnSO_4$ with EGTA, HEDTA and EDTA chelators) in a range of free Zn(II) concentration ($[Zn(II)]_{free}$ from 10^{-8} to $\sim 10^{-15}$ M (Tables S2, S3 and Fig. S6, ESI†).[34] Heterodimer formation was examined as a function of free Zn(II) concentration (Fig. 2D) and FRET was monitored to determine the heterodimer conditional binding constant K_{12} = [Zn(CD4RARH)(Lck)]/([Zn(II)]$_{free}$[CD4RARH][Lck]). The results of normalized fluorescence ratios of donor and acceptor indicate that 50% of the heterodimer is formed at $-\log[Zn(II)]_{free}$ (pZn) = 12.0 with K_{12} = 4×10^{18} M^{-2} at pH 7.4, with good convergence to the PAR experiment (Fig. 2E and Table S4, ESI†).[35] When Zn(II)-buffered media were applied for CD-monitored complex formation of the unlabeled variants, two separate events were observed with ellipticity change inflection points at pZn of 12.1 and 8.8 (Fig. 2F). The first isotherm corresponds to the heterodimer formation and the obtained K_{12} constant is highly convergent with that obtained from the FRET study. The second event has been assigned for Zn(CD4RARH)$_2$ homodimer formation (binding constant of 1×10^{14} M^{-2}), since it is more stable than Zn(Lck)$_2$ (see above, Fig. S1 and Table S4, ESI†). The value of conditional binding constant of the Zn(CD4RARH)$_2$ complex is comparable to other ZnL_2 complexes formed by Zn(II) coordination to CXXC or CXC peptide sequences that do not form specific interactions.[21] Such a huge difference in the stability of hetero- and homodimer species makes the homodimer presence negligible in non-buffered conditions. Results performed in free Zn(II)-controlled media clearly show the advantage of this system, where one is able to control protein assembly by changing Zn(II) availability. If this is not the aim, lack and full saturation are obtained in the absence and excess of Zn(II) ions in unbuffered media.

Zinc clasp-based toolset was utilized in approaches related to protein modification and purification by CD4RARH addition to the protein of interest (POI), the E3-binding domain of dihydrolipoamide succinyltransferase (BBL) from *E. coli*.[36] For this purpose CD4RARH peptide was synthesized as a functional tag using Dawson resin in the form of Dbz-peptide derivative.[37] POI with N-terminal cysteine was conjugated with CD4RARH-Dbz peptide using native chemical ligation (NCL) as presented in Fig. 3A. Rapid ligation of the mixture in the presence of 4-mercaptophenylacetic acid results in the ligated product, whose metal-response and heterodimerization properties were confirmed using CD spectroscopy and SEC (Fig. S7 and S8, ESI†).

To capture CD4RARH by the Zn(II)-dependent interaction, molecular baits based on the Lck domain were developed with

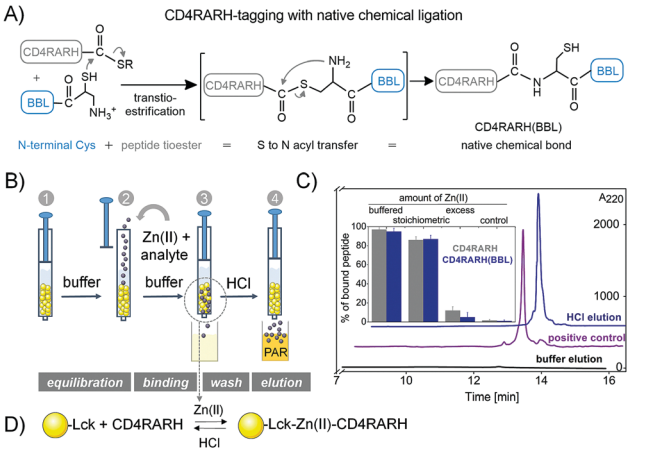

Fig. 3 (A) Scheme of native chemical ligation used for CD4RARH-tagging of BBL small protein domain. (B) Workflow of Lck-immobilized molecular bait (yellow), Zn(II)-dependent (grey), fishing with equilibration, binding, washing and elution steps. (C) HPLC chromatograms of buffer (black) and HCl (blue) elution samples along with the positive control (unmodified resin). Inset presents the percentage of CD4RARH (grey) and CD4RARH(BBL) (blue) bound to Lck-immobilized baits in a variable amount of Zn(II) (ESI†). (D) Capturing the reversible, Zn(II)-dependent interaction of Lck and CD4RARH on the solid support.

SPPS Fmoc synthesis and TFA-resistant TentaGel S NH_2 resin (Fig. 3B). Functionalized baits were incubated in HEPES buffer, supplemented with TCEP and 1.2 equivalents of Zn(II) over theoretical resin capacity. Peptide on-resin capacity (0.23 ± 0.04 mmol g^{-1}, $90 \pm 17\%$ synthesis efficiency) was examined by quantification of released Zn(II) with PAR chromophore after washing steps and acidification to pH 2 (Scheme S2, ESI†). Stability of functionalized resin was analytically determined for 6 months storage at 4 °C. Binding of CD4RARH and CD4RARH(BBL) was performed with different amount of Zn(II) and the efficiency was tested by HPLC analysis of eluted fractions with unmodified resin samples as a control (Fig. 3C). Zn(II)-buffered media (1 mM HEDTA with 0.8 mM $ZnSO_4$) indicated 97 and 95% level of CD4RARH and CD4RARH(BBL) binding, stoichiometric amount of Zn(II) (1.2 eq. of $ZnSO_4$ over CD4RARH) resulted in 86% and 87% and the excess of Zn(II) (1.2 eq. over Lck on-resin capacity) in 12% and 5%. Successful capture of CD4RARH and CD4RARH(BBL) conjugate to immobilized Lck showed the potential of the developed system to be used in both protein heterodimerization assembly and molecular biology routes.

To investigate kinetic parameters and emphasize specificity of binding the biolayer interferometry technique was employed for CD4RARH, CD4RARH(BBL), CD4RARH(Clover) and *E. coli* lysate with overexpressed CD4RARH(Clover) (Fig. 4A). Biotinylated Lck domain was synthesized by orthogonal functionalization (Scheme S1, ESI†) and immobilized on streptavidin biosensors to analyze the interference pattern of reflected light. The results of sequential association and dissociation steps are presented as normalized sensograms in Fig. 4B, where Zn(II)-dependence was reported by the HCl dissociation step. The specificity of binding was confirmed on the *E. coli* bacterial lysate with overexpressed

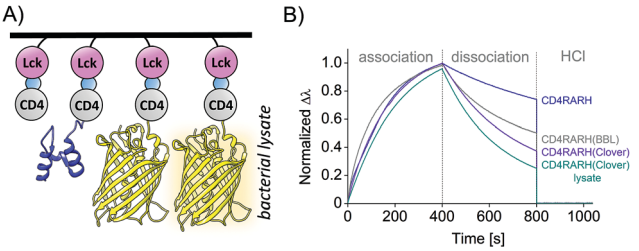

Fig. 4 (A) Zn(II)-mediated interaction of CD4RARH-tagged proteins with Lck monitored by bio-layer interferometry. (A) Graphical depiction of streptavidin biosensor with immobilized Lck (pink), Zn(II) (blue) and subsequently: CD4RARH, CD4RARH(BBL), CD4RARH(Clover) and *E. coli* lysate with overexpressed CD4RARH(Clover). (B) Normalized sensograms present binding kinetics of association and dissociation for indicated in (A) systems.

CD4RARH-Clover. Results were fitted to a 1:2 heterogeneous model for association (k_{on}) and dissociation (k_{off}) rate constants determination (Table S5 and Fig. S9, ESI†). High similarity of the association kinetics for all CD4RARH-tagged proteins was indicated. Therefore, the parameters for the dissociation process show a decreasing tendency with the increase of the conjugate mass, which is typical for applied technique.

Our study on the zinc clasp-based motif highlights the utilization of metal-driven interactions to develop reversible protein heterodimerization systems. Efficient formation of the compactly folded zinc clasp scaffold providing stability, specificity, and reversibility has been used to show its potential in protein modification and purification. Examination of Lck-based molecular baits indicates suitability of a tool to search for partners in a wide range of cellular Zn(II)-dependent interaction networks. A novel protein heterodimerizer enriches and expands the utility of the metal-based interfaces as well as metal-driven protein–protein interactions not only in protein engineering but also in molecular biology and nanotechnology.

The study was sponsored by the National Science Centre of Poland, grants no. 2012/07/E/NZ1/01894 and 2014/13/B/NZ1/00935 (to A. Krężel).

Conflicts of interest

There are no conflicts to declare.

Notes and references

1 A. Fegan, B. White, J. Carlson and C. Wagner, *Chem. Rev.*, 2010, **110**, 3315–3336.
2 M. Long, J. Poganik and Y. Aye, *J. Am. Chem. Soc.*, 2016, **138**, 3610–3622.
3 D. Bondeson, A. Mares, I. Smith, E. Ko, S. Campos, A. Miah, K. Mulholland, N. Routly, D. Buckley and J. Gustafson, *et al.*, *Nat. Chem. Biol.*, 2015, **11**, 611–617.
4 H. Lin, J. Haegele, M. Disare, Q. Lin and Y. Aye, *J. Am. Chem. Soc.*, 2015, **137**, 6232–6244.
5 J. Ali, A. Jackson, A. Howells and A. Maxwell, *Biochemistry*, 1993, **32**, 2717–2724.
6 H. Lin, W. Abida, R. Sauer and V. Cornish, *J. Am. Chem. Soc.*, 2000, **122**, 4247–4248.
7 L. Banaszynski, C. Liu and T. Wandless, *J. Am. Chem. Soc.*, 2005, **127**, 4715–4721.
8 R. Freiberg, D. Spencer, K. Choate, P. Peng, S. Schreiber, G. Crabtree and P. Khavari, *J. Biol. Chem.*, 1996, **271**, 31666–31669.
9 S. Rowe, R. Casey, B. Brennan, S. Buhrlage and A. Mapp, *J. Am. Chem. Soc.*, 2007, **129**, 10654–10655.
10 C. Fellmann and S. Lowe, *Nat. Cell Biol.*, 2014, **16**, 10–18.
11 P. McEnaney, K. Fitzgerald, A. Zhang, E. Douglass, W. Shan, A. Balog, M. Kolesnikova and D. Spiegel, *J. Am. Chem. Soc.*, 2014, **136**, 18034–18043.
12 L. Xu, M. Sun, W. Ma, H. Kuang and C. Xu, *Mater. Today*, 2016, **19**, 595–606.
13 C. Rollins, V. Rivera, D. Woolfson, T. Keenan, M. Hatada, S. Adams, L. Andrade, D. Yaeger, M. van Schravendijk and D. Holt, *et al.*, *Proc. Natl. Acad. Sci. U. S. A.*, 2000, **97**, 7096–7101.
14 I. Serafimova, M. Pufall, S. Krishnan, K. Duda, M. Cohen, R. Maglathlin, J. McFarland, R. Miller, M. Frödin and J. Taunton, *Nat. Chem. Biol.*, 2012, **8**, 471–476.
15 B. Vallee and D. Auld, *Biochemistry*, 1990, **29**, 5647–5659.
16 W. Maret, *Adv. Nutr.*, 2013, **4**, 82–91.
17 A. Krężel and W. Maret, *Arch. Biochem. Biophys.*, 2016, **611**, 3–19.
18 A. W. Song, P. Sontz, X. Ambroggio and F. Tezcan, *Annu. Rev. Biophys.*, 2014, **43**, 409–431.
19 J. Brodin, X. Ambroggio, C. Tang, K. Parent, T. Baker and F. Tezcan, *Nat. Chem.*, 2012, **4**, 375–382.
20 M. Murakami and T. Hirano, *Cancer Sci.*, 2008, **99**, 1515–1522.
21 T. Kochańczyk, M. Nowakowski, D. Wojewska, A. Kocyła, A. Ejchart, W. Koźmiński and A. Krężel, *Sci. Rep.*, 2016, **6**, 36346.
22 T. Kochańczyk, P. Jakimowicz and A. Krężel, *Chem. Commun.*, 2013, **49**, 1312–1314.
23 M. Merkx, M. Golynskiy, L. Lindenburg and J. Vinkenborg, *Biochem. Soc. Trans.*, 2013, **41**, 1201–1205.
24 V. Cangelosi, A. Deb, J. Penner-Hahn and V. Pecoraro, *Angew. Chem., Int. Ed.*, 2014, **126**, 8034–8037.
25 M. Zastrow, A. Peacock, J. Stuckey and V. Pecoraro, *Nat. Chem.*, 2011, **4**, 118–123.
26 K. Kirkbride, B. Ray and G. Blobe, *Trends Biochem. Sci.*, 2005, **30**, 611–621.
27 P. W. Kim, Z. Y. Sun, S. C. Blacklow, G. Wagner and M. J. Eck, *Science*, 2003, **301**, 1725–1728.
28 A. Kocyła, J. Adamczyk and A. Krężel, *Metallomics*, 2018, **10**, 120–131.
29 A. Davis and J. Berg, *J. Am. Chem. Soc.*, 2009, **131**, 11492–11497.
30 A. Ozbabacan, H. B. Engin, A. Gursoy and O. Keskin, *Protein Eng., Des. Sel.*, 2011, **24**, 635–648.
31 A. Kocyła, A. Pomorski and A. Krężel, *J. Inorg. Biochem.*, 2015, **152**, 82–92.
32 K. Kluska, J. Adamczyk and A. Krężel, *Coord. Chem. Rev.*, 2018, **367**, 18–64.
33 B. A. Krizek, D. L. Merkle and J. M. Berg, *Inorg. Chem.*, 1993, **32**, 937–940.
34 A. Lam, F. St-Pierre, Y. Gong, J. Marshall, M. McKeown, M. Schnitzer, R. Tsien and M. Lin, *Biophys. J.*, 2013, **104**, 683a.
35 A. Pomorski, T. Kochańczyk, A. Miłoch and A. Krężel, *Anal. Chem.*, 2013, **85**, 11479–11486.
36 H. Neuweiler, T. Sharpe, T. Rutherford, C. Johnson, M. Allen, N. Ferguson and A. Fersht, *J. Mol. Biol.*, 2009, **390**, 1060–1073.
37 J. Blanco-Canosa and P. Dawson, *Angew. Chem., Int. Ed.*, 2008, **120**, 6957–6961.

